



## OPEN ACCESS

## EDITED BY

Abdoulaye Doucouré,  
Donyatek, Strategic Planning and Professional  
Development, United States

## REVIEWED BY

Gyorgy Szekely,  
King Abdullah University of Science and  
Technology, Saudi Arabia  
Jegatha Nambi Krishnan,  
Birla Institute of Technology and Science, India

## \*CORRESPONDENCE

Heidi Lynn Richards,  
✉ heidi.richards@wits.ac.za

RECEIVED 05 February 2025

ACCEPTED 28 April 2025

PUBLISHED 14 May 2025

## CITATION

Maziya K, Kotze I and Richards HL (2025)  
Enhancing dye rejection and antifouling  
resistance of thin film nanocomposite  
nanofiltration membranes by the incorporation  
of glutamic acid functionalized graphene oxide.  
*Front. Membr. Sci. Technol.* 4:1571459.  
doi: 10.3389/frmst.2025.1571459

## COPYRIGHT

© 2025 Maziya, Kotze and Richards. This is an  
open-access article distributed under the terms  
of the [Creative Commons Attribution License  
\(CC BY\)](https://creativecommons.org/licenses/by/4.0/). The use, distribution or reproduction in  
other forums is permitted, provided the original  
author(s) and the copyright owner(s) are  
credited and that the original publication in this  
journal is cited, in accordance with accepted  
academic practice. No use, distribution or  
reproduction is permitted which does not  
comply with these terms.

# Enhancing dye rejection and antifouling resistance of thin film nanocomposite nanofiltration membranes by the incorporation of glutamic acid functionalized graphene oxide

Khona Maziya, Izak Kotze and Heidi Lynn Richards\*

Molecular Sciences Institute, School of Chemistry, University of the Witwatersrand, Johannesburg, South Africa

To enhance membrane performance of nanofiltration (NF) membranes for dye wastewater treatment, thin film nanocomposite (TFN) membranes embedded with glutamic acid brush modified graphene oxide (GO-GLU) were fabricated. In this current study, GO-GLU was introduced to the selective polyamide (PA) layer which was prepared via interfacial polymerization of organic trimesoyl chloride (TMC) and aqueous m-phenylenediamine (MPD) on a polysulfone (PSF) support. Water permeability and dye rejection with methyl orange (MO) and methylene blue (MB) were used to evaluate membranes performance. The evaluation of TFN membranes via WCA, FTIR, SEM, and AFM demonstrated that GO-GLU nanosheets enhanced hydrophilicity. The fabricated GO-GLU TFN membrane attained a water permeance of 14.11 L/m<sup>2</sup>h at the optimal GO-GLU dosage of 0.10 wt%, with 99.18% MB rejection and 67.18% MO rejection. Furthermore, it displayed superior antifouling characteristics against Bovine Serum Albumin (BSA) than the virgin TFC membrane and potentially good operation stability performance after 3 cycles. The results proved that addition of GO-GLU nanosheets enhanced membrane performance. The TFN membranes provide excellent performance in effectively removing of dyes from both synthetic and river water samples, rendering them a suitable alternative for wastewater treatment. The study sheds fresh light on the construction of NF membranes by using GO-GLU nanosheets to boost the membranes hydrophilicity and antifouling properties.

## KEYWORDS

Thin film nanocomposite membranes, graphene oxide, glutamic acid, dyes, antifouling

## 1 Introduction

The growing contamination of water sources with harmful organic compounds discharged by the textile and dyeing industries is a worldwide concern. Due to their widespread use in the textile industry, untreated dye wastewater is one of the leading causes of water pollution (Wu et al., 2021). Synthetic dyes including methyl orange (MO) and methylene blue (MB) have been found in textile wastewater. MB is a cationic dye containing adjacent aromatic rings that is utilized in the dyeing of cotton and wool. MO, on the other

hand, is an anionic dye with a double bond  $N=N$  in its structure that is commonly utilized in printing, textile, and pharmaceutical sectors (Shakya et al., 2019). Even in low concentrations, these hues in bodies of water are highly visible and have serious adverse effects (Shakya et al., 2019; Nikoee and Saljoughi, 2017). One of the main effects is a reduction in sunlight infiltration, which negatively influences photosynthesis in living organisms and, as a result, the rate of dissolved oxygen (Yagub et al., 2014; Bangari et al., 2022). Furthermore, prolonged direct contact with this pollutant class may be detrimental, resulting in digestive, liver, cancer, and other health problems since they are persistent and bioaccumulate in living organisms (Pramono et al., 2023; Li et al., 2017).

In order to eliminate dyes from wastewater, physical, biological, and chemical approaches have been examined (Moradihamedani, 2022). However, membrane separation techniques have been favored for the removal of dyes from water sources owing to their multiple benefits such as cost effectiveness, environmental friendliness, excellent removal efficacy as well as low energy consumption (Moradihamedani, 2022; Liao et al., 2021). Among various membranes, thin film nanocomposite (TFN) membranes prepared using interfacial polymerization (IP) technique on a porous support have demonstrated a high efficacy in the removal of dyes in water (Mansourpanah et al., 2021; Zhao P. et al., 2019; Wang et al., 2022; Mousavi et al., 2020). Ormanci-Acar et al. (2018) studied dye removal efficacy of TFN membranes containing halloysite nanotubes (HNTs). In their investigation, HNTs were added to the organic phase during IP to create nanofiltration (NF) membranes that had excellent pH and temperature tolerance (Ormanci-Acar et al., 2018). Filtration performance experiments were performed using dyes, NaCl and  $MgSO_4$  solutions (Ormanci-Acar et al., 2018). At 0.04 wt% of HNTs,  $MgSO_4$ , NaCl, Reactive orange and Setazol red reactive dyes were rejected at 94.4%, 49%, 99.7%, and 99.7%, respectively (Ormanci-Acar et al., 2018). Yang et al. (2022) studied the effects of polydopamine functionalized cellulose nanocrystals (CNCs) TFN membranes for the removal of dye and salt from textile effluent. The TFN membranes displayed exceptional salt permeability of 99.33%, an excellent Congo red (CR) removal of 99.91%, and an outstanding pure water permeability (PWP) of 128.4 LMH  $bar^{-1}$  (Yang et al., 2022).

TFN membranes are characterized by the inclusion of nanofillers in the polyamide (PA) layer which enhance selectivity, antifouling properties, and water flux. The choice of nanofiller is critical to the TFN membranes' fabrication. Unique nanofillers such as halloysite nanotubes (HNTs), cellulose nanocrystals, carbon nanotubes, graphene quantum dots, and metallic organic frameworks (MOFs) have been introduced to the PA layer to boost the membranes' performance (Mousavi et al., 2020; Ormanci-Acar et al., 2018; Bi et al., 2018; Zhang et al., 2021; Yang et al., 2023; Ma et al., 2017; Ge et al., 2024). Graphene oxide (GO) has recently attracted a lot of attention due to its several appealing properties, such as its large specific surface area ( $\sim 2600 \text{ m}^2\text{g}^{-1}$ ), hydrophilic nature, and the presence of epoxy, ketones, carboxyl and hydroxyl groups. These allow for further functionalization of GO, thereby improving contaminant removal (Peng et al., 2016; Gopalakrishnan et al., 2015; Li et al., 2021). Several studies have been reported where GO was used to boost membrane performance (Kang et al., 2019; Lin et al., 2020; Abadikhah et al., 2019a; Abadikhah et al., 2019b; Izadmehr et al., 2020; Zhao et al.,

2023; Li et al., 2019; Tang et al., 2023; Zhang et al., 2017; Jee et al., 2022). Examined the impact of GO quantum dots (GQDs) on the performance of the membrane (Zhao G. et al., 2019). The GQDs were embedded into the TFN PA layer via surface coating, and membrane rejection against MO and MB dyes was assessed (Zhao G. et al., 2019). MO rejection increased from 89.2% to 97% after PA layer modification with GQDs due to electrostatic repulsion (Zhao G. et al., 2019). There was a decrease in MB rejection (75.4%–71%), ascribed to the adsorption of positively charged MB onto the membrane, thus reducing water flux and rejection (Zhao G. et al., 2019).

However, two key issues impede the usage of GO-functionalized membranes in water treatment to date. Agglomeration of GO at high concentrations affects membrane performance and also decreases the membranes water flux and hydrophilicity. Secondly, the stacking of GO nanosheets limits the movement of water through the membrane thus reducing the its permeability (Nair et al., 2012; Anand et al., 2018; Feng et al., 2022). Therefore, in an effort to improve membrane performance, it is crucial to address these issues by modifying GO nanosheets via attaching various functional groups prior to membrane fabrication. Seah et al. (2022) examined the effects of modified GO TFN membranes on salt/dye removal. Accordingly, they prepared a PA layer using a mist-based IP approach in order to fabricate TFN membrane with improved characteristics. GO was modified with Acrylic acid (AA) by plasma-enhanced chemical vapor deposition (Seah et al., 2022). The acrylic acid-modified GO increased the PWP of TFN membranes by 6.6%, attaining 11.34  $L/m^2h\text{-bar}$  compared to the control GO TFN. These membranes were comparatively assessed for Rhodamine B, Acid Red, and Rose Bengal dye rejection, achieving rejection rates of more than 98% (Seah et al., 2022). Modification of GO to overcome these shortcomings is crucial, since it also enhances water permeability, dye removal, thermal and mechanical stabilities, and antifouling properties. One of the strategies that can be explored is polymerization that involves taking advantage of the functional groups that contain oxygen on the surface of GO to enhance interlayer spacing of the GO sheets which also allows for holding together of the sheets. GO modification via surface-initiated atom transfer radical polymerization (SI-ATRP) is a flexible polymerization technique that results in high grafting density and control over the brushes architecture and thickness. This method involves immobilizing an initiator on the substrates surface, subsequent to the growth phase through the repetitive addition of monomers on the growing chain (polymerization) (Azzaroni, 2012; Zhao and Zhu, 2009). This functionalization results in multifunctional materials with end group functionalities (Keating et al., 2016).

In this study, we present the synthesis of GLU polymerized GO (GO-GLU) via SI-ATRP and its subsequent inclusion into TFN membranes for the rejection of MO and MB dyes in water. The incorporation of GO-GLU nanosheets represents an innovative modification of the PA layer, leveraging the functional properties of GO combined with GLU brushes. This functionalization improves water flux, dye rejection efficiency, and antifouling characteristics while maintaining membrane stability over multiple cycles at low operational pressure. The study also evaluates performance against environmental samples (river water), showcasing practical applicability.

## 2 Materials and methods

### 2.1 Materials

Graphite powder, ethanol (CH<sub>3</sub>-CH<sub>2</sub>-OH), diethyl ether (CH<sub>3</sub>-CH<sub>2</sub>-O-CH<sub>2</sub>-CH<sub>3</sub>), phosphoric acid (H<sub>3</sub>PO<sub>4</sub>), methylene blue (C<sub>16</sub>H<sub>18</sub>ClN<sub>3</sub>S), potassium permanganate (KMnO<sub>4</sub>), α-bromoisobutyryl bromide (BiBB) (98%), hydrogen peroxide (H<sub>2</sub>O<sub>2</sub>), chloroform, methanol (CH<sub>3</sub>OH), tetrahydrofuran (THF), dimethylformamide (DMF), polysulphone (PSF) pellets (MW = 35 K g/mol), trimesoyl chloride (TMC), glutamic acid, N,N,N,N,N'-pentamethyldiethylenetriamine (PMDETA, 99%), sulphuric acid (H<sub>2</sub>SO<sub>4</sub>), methyl orange (C<sub>14</sub>H<sub>14</sub>N<sub>3</sub>NaO<sub>3</sub>S), triethylamine (TEA, 99%), m-phenylenediamine (MPD), copper(I) bromide (CuBr) and Polyvinylpyrrolidone (PVP) (Mw = 30–70 K; 87%–90%) were obtained from Sigma-Aldrich. De-ionized (DI) water possessing a resistance of 18 mΩ cm was used in all experiments (Milli-Q system, Millipore).

### 2.2 GO nanosheets synthesis

GO was synthesized by the improved Hummers method (Marcano et al., 2018). Briefly, graphite powder (1 g) followed by KMnO<sub>4</sub> (6 g) was added to a concentrated mixture of H<sub>2</sub>SO<sub>4</sub> and H<sub>3</sub>PO<sub>4</sub> in a 9:1 ratio. For 12 h, the mixture was stirring in an oil bath set to 50°C. After the reaction was completed, it was allowed to cool to ambient temperature before being transferred to 400 mL of ice with 1 mL of 30% hydrogen peroxide (H<sub>2</sub>O<sub>2</sub>). When the mixture had reached room temperature, it was centrifuged at 4,000 rpm for 30 min and the supernatant was carefully decanted. The precipitate was washed twice with DI water before being rinsed with 30% HCl and ethanol. After this thorough washing, the residual material was coagulated with 200 mL diethyl ether. The resulting solid was then placed under vacuum and dried overnight at ambient temperature. Finally, the dried solid was pulverized with a mortar and pestle.

### 2.3 Synthesis of initiator-attached GO (GO-Br)

The modification of GO was performed using an altered approach described by Kumar et al. (2016). To prepare the colloidal suspension, typically, GO was placed in a round-bottom flask comprising of 30 mL DMF and subjected to sonication for an hour. After adding TEA (4 mL) to the flask, BIBB was gradually added to the mixture which was stirred in an ice bath (24 h). GO-Br was recovered using centrifugation and washed with chloroform and DI water prior to being vacuum dried for 12 h.

### 2.4 SI-ATRP of glutamic acid on initiator attached GO (GO-Br)

The polymerization of GO-Br was performed using a modified approach described by Kumar et al. (2016). Briefly, sonication was

TABLE 1 TFN membranes GO-GLU 100 loading.

Membrane	GO-GLU 100 loading (wt%)
TFC	-
TFN-1	0.025
TFN-2	0.05
TFN-3	0.10

used to disperse 50 mg GO-Br in DMF. Cu(I)Br (0.2 mmol) with various quantities of glutamic acid (50, 100, and 200 mmol) was placed into sealed vials and degassed using nitrogen purging. To the reaction mixture, 0.2 mmol of PMDETA (ligand) was added, followed by 24 h of polymerization at 70°C. Methanol was utilized to precipitate polymer composites by pouring reaction mixture to it. To remove the occluded monomer, the product (GO-GLU 50/100/200) was washed numerous times with chloroform, centrifuged, and vacuum dried for 24 h.

### 2.5 Membrane synthesis

#### 2.5.1 Polysulfone (PSF) support preparation

The PSF substrate was produced through the phase inversion technique. To make the PSF membrane casting solution, 1 wt% PVP and 16 wt% PSF were allowed to dissolve in DMF solvent. To ensure homogeneity, the solution was stirred for 12 h at 50°C. To perform solvent/non-solvent exchange (wet phase inversion), the solution was degassed, cast on a glass plate with a thickness of 100 μm, and submerged in a water coagulation bath at ambient temperature. The electrometer 4843 automatic film applicator (Manchester, United Kingdom) was used for casting. To eliminate any remaining DMF, the membranes were washed with fresh distilled water and then stored in distilled water until use.

#### 2.5.2 Preparation of polyamide (PA) selective layer

The membranes' PA layer was synthesized atop a PSF support membrane employing the traditional interfacial polymerization (IP) process. Pre-treatment of the PSF support membranes involved soaking them in an overnight solution of 0.5% sodium dodecyl sulphate (SDS). After that, membranes were rinsed for an hour with distilled water. The PSF membrane was then secured between a glass plate and a frame. A 20 mL aqueous solution containing 2 w/v% MPD was poured onto the porous substrate. Following a 2-min contact period, surplus MPD solution was eliminated from the surface by vertically positioning it for 1 min. The PSF substrate was then exposed to an organic phase containing a 0.2 wt% TMC-hexane solution for a minute before being removed from the membrane surface. To increase crosslinking, the treated membrane was dried for 8 min at 60°C before being rinsed with distilled water. The fabrication technique of GO-GLU TFN membranes resembled that used for TFC membranes, with the exception that GO nanosheets (modified) were first added to an aqueous solution of MPD (Table 1). Prior to interfacial polycondensation reaction, all MPD/additives solutions were sonicated for 30 min (Masibi et al., 2022).

## 2.6 Characterization

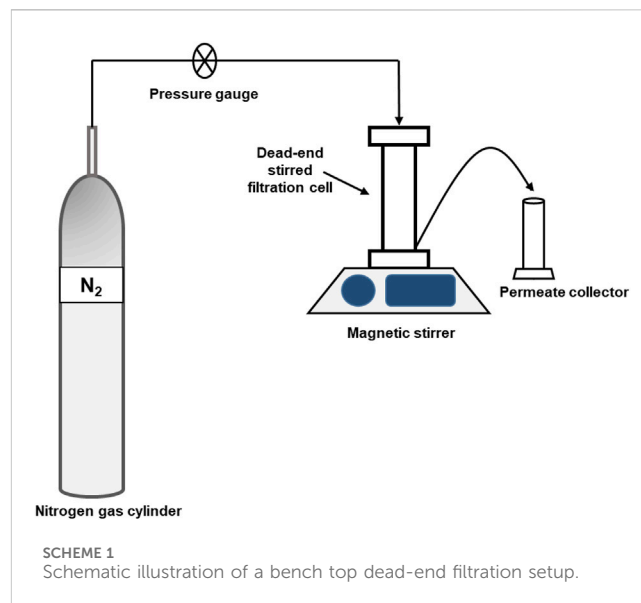
An FEI Tecnai G2 Spirit transmission electron microscope (Hillsboro, United States) with a 120 kV acceleration voltage was utilized to study the morphological characteristics of GO nanosheets. Bruker D2 phaser diffractometer (Cu-K $\alpha$ ) (Johannesburg, South Africa) was utilized for X-ray diffraction investigations, with a scanning range of 5–90 (2 $\theta$ ). A Tensor 27 Infrared Spectrometer (Massachusetts, United States) was employed to acquire Fourier transform infrared (FTIR) spectra ranging from 500 to 4000 cm<sup>-1</sup> for the GO nanosheets and membranes (OPUS software). The magic-angle solid state <sup>13</sup>C nuclear magnetic resonance (<sup>13</sup>C MAS NMR) spectra of GO and GO-GLU were recorded on an AVANCE-III-500 (Bruker, Germany) machine. Direct polarization high power broad band <sup>1</sup>H decoupling and Cross-polarization MAS was acquired using 4 mm zirconium rotors with 8 or 10 kHz MAS spin-rate. <sup>13</sup>C NMR chemical shifts were externally referenced with adamantane as described by Hoffman (2022). VarioELcube v4.0.13 (Elementar, Germany) was used for elemental study of carbon, hydrogen, nitrogen, and sulfur (CHNS). The thermal properties of GO and its derivatives was studied using thermogravimetric analysis (TGA), which was performed in an inert (nitrogen) environment on a thermogravimetric analyzer through a temperature ranging from 35°C–900°C (heating rate = 20 °C/min) (Perkin Elmer). Cross-sectional and surface morphologies of the produced membranes were studied by means of scanning electron microscopy (SEM-EDS) (Tescan Vega). TFN membranes were initially coated (carbon and Pd/Au) and examined under SEM (accelerating voltage = 20 kV). To assess membranes hydrophilicity, contact angle instrument (DataPhysics Instruments GmbH, Filderstadt, Germany) was used to measure the contact angles using the sessile-drop method. Each membrane sample (dried) was measured ten times at various regions using the sessile-drop method.

GO and derivatives' pH point of zero charge (pH PZC) was obtained through the use the salt titration method (Eitale et al., 2021). Briefly, 0.1 g of GO-GLU 100 was placed in five polypropylene tubes containing 25 mL of 0.01M NaCl. The pH of these solutions was then altered between 2–10 with 0.1 M HNO<sub>3</sub> as well as 0.1 M NaOH, giving each one a unique pH value. The suspensions were shaken horizontally for 24 h. Each solution's final pH was plotted against its original pH, and the material's pH PZC was derived using the intersection points (Eitale et al., 2021).

## 2.7 Water intake capacity (WIC)

The weight difference between the dry and wet TFC and TFN membranes was used to calculate WIC. To determine the dry weight ( $W_d$ ), the membranes were oven-dried to remove any moisture thereafter weighed before being placed in distilled water (24 h). The saturated membranes were gently patted prior to weighing to ascertain their wet weight ( $W_w$ ) (Equation 1).

$$\text{WIC (\%)} = (W_w - W_d) / W_d \times 100 \quad (1)$$



## 2.8 Membrane performance

The performance of all developed membranes was assessed by the use of a dead-end filtration system that is nitrogen-pressure driven (HP4750 Stirred Cell, Sterlitech) (Scheme 1). Membranes having an area of 0.00146 m<sup>2</sup> were compacted with DI water (transmembrane pressure = 600 kPa) until a steady flow was achieved. Equation 2 was employed to compute the pure water flux at a pressure of 300 kPa with DI water as the feed solution.

$$J_w = Q / (A \cdot \Delta t) \quad (2)$$

Where by: Q is the volume of permeated water (L); A is the membrane's effective area (m<sup>2</sup>),  $\Delta t$  is the permeation time (h) and  $J_w$  is the pure water flux (L/m<sup>2</sup>h);

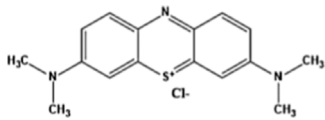
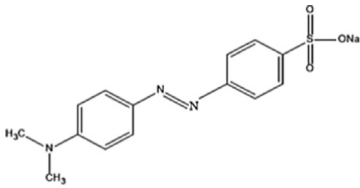
A dead-end filtering cell was employed for dye rejection tests (single component), with continual magnetic stirring (Scheme 1). Two organic dyes of different electrostatic charges were used; Methyl orange (MO) and Methylene blue (MB) (Table 2). At 300 kPa, varying dye concentrations (20, 50, 80, 100 mg/L) and pH (2–7–11) were investigated (single component), these were run through the cell. River water samples were collected from South Africa's Vaal River to evaluate the potential use of the TFN membrane in environmental water systems. The physicochemical characteristics of the water samples were as follows: conductivity 834  $\mu$ S/cm, pH 7.61, total dissolved solids (TDS) 417 ppm, and resistivity 1.20 k $\Omega$  cm. The water samples were spiked with MB dye (50 mg/L). The change of the concentration of the MB and MO solution was monitored by means of UV–visible (UV–vis) spectroscopy at 664 and 464 nm, respectively.

The measured rejection (%R) was determined using Equation 3:

$$\%R = \left(1 - \left(C_p / C_f\right)\right) \times 100 \quad (3)$$

where  $C_f$  and  $C_p$  denote the dye concentrations (mg/L) of the feed and permeate solutions.

TABLE 2 The molecular structure, weight and charge of the dyes.

Dyes	MB	MO
Molecular structure		
Charge	+	-
Molecular weight (MW) (g/mol)	319.85	327.33

## 2.9 Antifouling studies

BSA protein solution (concentration = 1 g/L; pH = 7) was employed to evaluate the membranes fouling characteristics. Firstly, the pure water flux ( $J_{po}$ ) was determined at a pressure of 300 kPa over a duration of 120 min. The pure water was subsequently substituted with the BSA solution and the permeate flow ( $J_{pt}$ ) was measured every 15-min for 120 min. The BSA solution was then substituted with pure water and the flux ( $J_{pf}$ ) was measured again for 120 min. The following equations (Equations 4–7) were used to determine the total fouling ratio (Rt), irreversible flux decline ratio (Rir), reversible flux decline ratio (Rr), and flux recovery ratio (FRR):

$$FRR (\%) = J_{pf} / J_{po} \times 100 \quad (4)$$

$$Rt (\%) = (J_{po} - J_{pt}) / J_{po} \times 100 \quad (5)$$

$$Rir (\%) = (J_{po} - J_{pf}) / J_{po} \times 100 \quad (6)$$

$$Rr (\%) = (J_{pf} - J_{pt}) / J_{po} \times 100 \quad (7)$$

## 3 Results and discussion

### 3.1 Morphology of GO nanocomposites and membranes

Figure 1 reveals the morphological investigation of the GO nanocomposites using TEM. Pristine GO and GO-Br images revealed smooth, thin and lamellar structure ranging from nano to micron scale nanosheets. Figure 1b displayed no observable difference in the morphology of the nanosheets after modification with ATRP initiator  $\alpha$ -bromoisobutryl bromide. However, in Figures 1c,d, GO is covered with nanosized poly (glutamic acid) brushes which are homogeneously spread on the surface of GO. This is due to the collapsed chains on the surface of the GO sheets resulting in nanosized spots (Zhu et al., 2012; Yang et al., 2009). With the increase in the grafting amount of glutamic acid, there is an observable increase in the sizes of dark spots and the aggregation of these (Figure 1). EDS analysis of GO-Br was carried out (Supplementary Figure S1). The EDS analysis of GO-Br verified the presence of C, O and Br at 0.27, 0.52, and 1.48 keV respectively, confirming the attachment of the Br containing initiator to the GO.

### 3.1.1 Membrane morphology and AFM analysis

Figure 2 depicts the synthesized membranes' surface and cross-sectional morphologies. The pure PSF membrane (Figures 2a,b) produced via phase inversion has an asymmetric spongy-like architecture comprising of a dense skin layer and a porous sub-layer. During phase inversion, the cast PSF polymer solution on a glass plate is immersed into a non-solvent bath (i.e., water) resulting in a rapid non-solvent/solvent replacement across the interface of non-solvent and casting film. Moreover, repulsive forces amid polymer and water sped up the precipitation of polymeric solution at the interface leading to the development of sub layer macro-voids and typical asymmetric structure together with a dense surface containing micro-pores (Hebbar et al., 2018; Cristina et al., 2020). The PSF support was used due to its favorable properties, which are crucial for enhancing membrane performance. The PSF material exhibits superior chemical and thermal stability, enabling it to operate effectively across a wide range of temperatures and pH levels, as well as demonstrating excellent resistance to chlorine (Cristina et al., 2020). The cross sections morphology for all the membranes are similar exhibiting asymmetric structure that comprises of a macro-void containing porous sub-layer and a dense top layer (Figures 2b,d,g,j,m). Upon IP, the surface morphology of TFC and TFN membranes displayed dense surfaces with the isolated distributed protrusions (Figures 2c,f,i,l). At lower nanoparticle concentrations, the TFN membranes were similar to TFC membrane signifying that the nanoparticles produced no significant effect on the surface morphology of the TFN membranes. However, nanoparticles aggregated as concentrations increased. (Figure 2l) (Shao et al., 2019).

Surface roughness for TFN membranes investigations were conducted using AFM analysis as presented in Figure 2. As shown, the membrane surface structures are depicted as bright and dark areas, representing the peaks and valleys, respectively. As displayed in Figures 2e,h,k,n, the TFC membrane displayed a rougher surface ( $Sa = 122$  nm) compared to other membranes (103–116 nm). Lower concentrations of nanoparticles in the PA layer result in decreased surface roughness. This might be caused by the inclusion of hydrophilic nanofiller, which may increase the compatibility of organic and aqueous phases during IP (Xie et al., 2017). In principle, membrane surfaces with low roughness and high hydrophilicity are expected to offer better fouling resistance (Natesan and GO, 2023). On the other hand, there was an observed slight increase of roughness at TFN-3, and this could be attributed to surface-located clusters caused by the agglomeration of

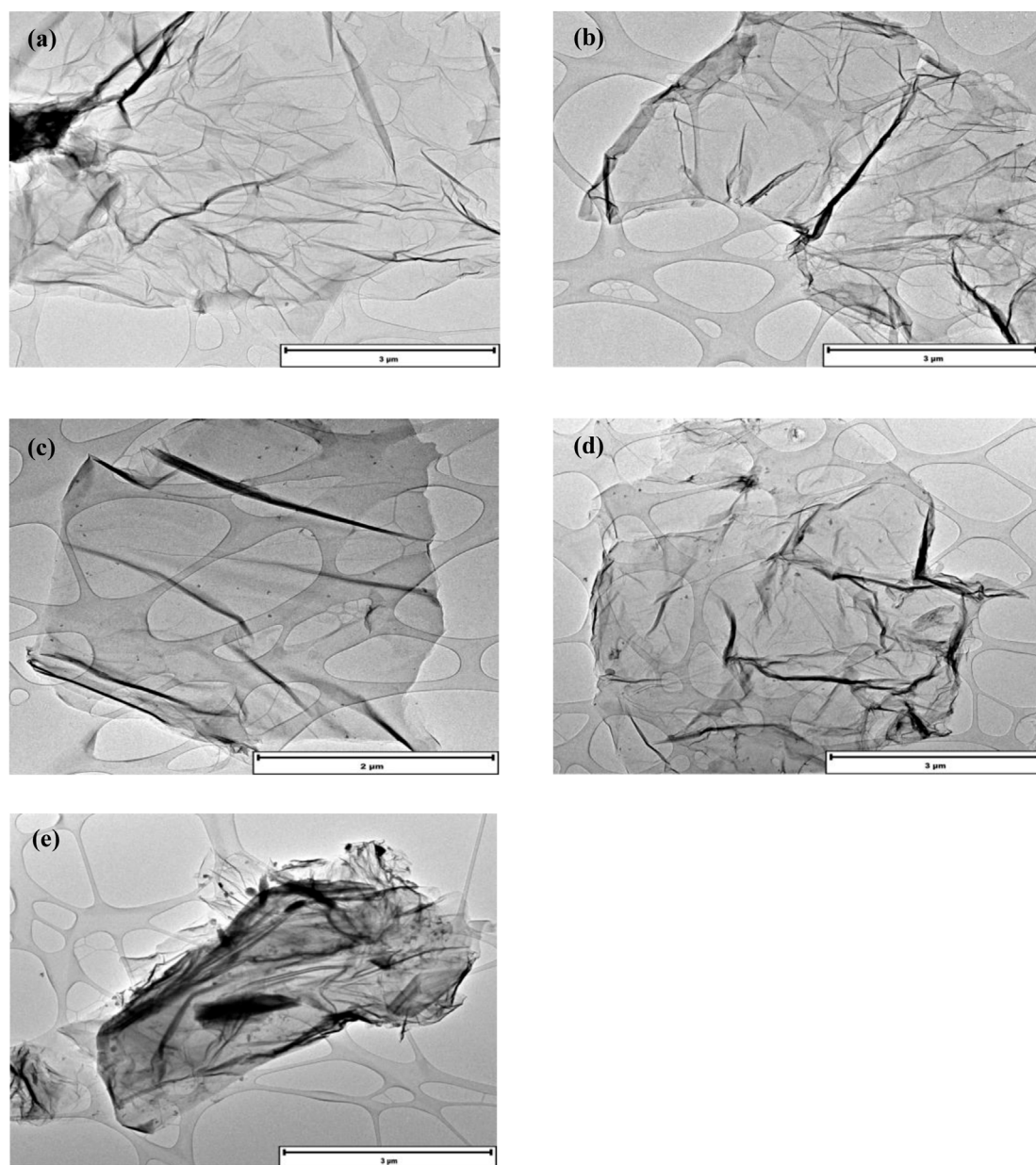


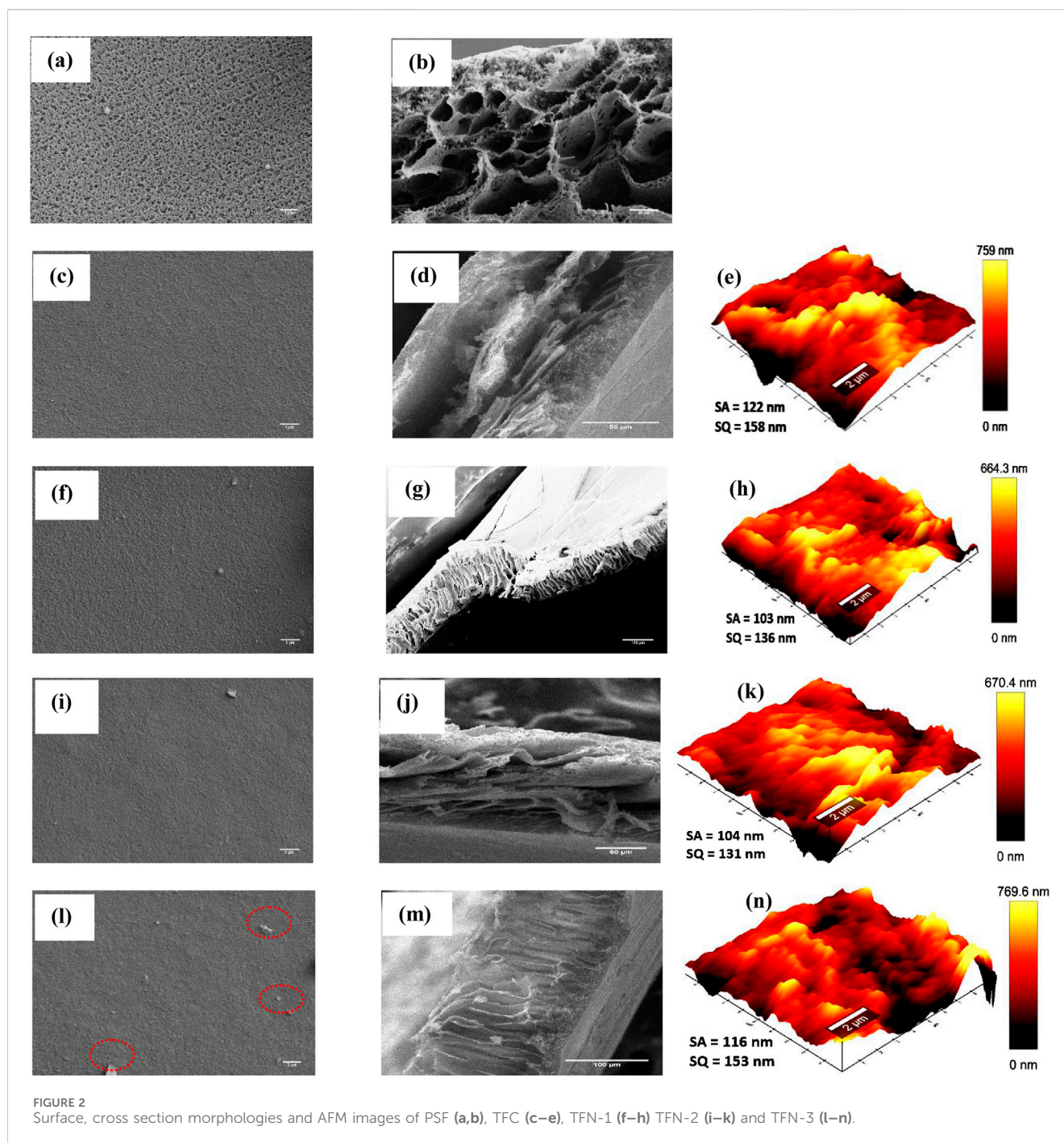
FIGURE 1  
TEM images of pristine GO (a), GO-Br (b), GO-GLU 50 (c), GO-GLU 100 (d) and GO-GLU 200 (e).

the GO. The morphological variation detected by AFM correlated with the SEM findings.

### 3.2 FTIR and elemental analysis of GO nanocomposites and membranes

Figure 3 illustrate the chemical transformation of GO, GO-Br and GO-GLU as confirmed by FTIR analysis. FTIR spectrum of pristine GO indicate a prominent peak at  $3321\text{ cm}^{-1}$ , indicative of the stretching vibrations of OH groups present in GO (Figure 3a). The GO spectrum additionally displayed peaks at  $2978\text{ cm}^{-1}$  credited to  $\text{CH}_2$ ,  $1737\text{ cm}^{-1}$  attributed to the stretching vibration of  $\text{-C=O}$  bond from the carboxylic group,  $1611\text{ cm}^{-1}$  corresponds to

the presence of unoxidized  $\text{sp}^2\text{ C=C}$  bond in the graphitic lattice structure,  $1420\text{ cm}^{-1}$  ascribed to the C-OH,  $1226\text{ cm}^{-1}$  linked to stretching vibrations of C-O group, and  $1027$  and  $863\text{ cm}^{-1}$  may be ascribed to epoxy groups (Hu et al., 2015). Following the modification of GO with the ATRP initiator BIBB, there was a decrease in O-H signal signifying that the O-H groups on GO's surface underwent esterification with the initiator (Figure 3a). The substitution of the C-OH and C-O-C peaks of GO with a new peak at about  $1180\text{ cm}^{-1}$  may be ascribed to the stretching vibrations of esters' C-O. In Figure 3b, the GO-GLU 100 displayed peaks at  $1714\text{ cm}^{-1}$  which correspond to the stretching vibration of  $\text{-C=O}$  bond due to the presence of the carboxylic group in glutamic acid. Other peaks include  $1570\text{ cm}^{-1}$  for the N-H bend,  $1371$  and  $1131\text{ cm}^{-1}$  corresponds to the  $\text{-C-N-}$  stretching in the



secondary amide groups which confirms the amidation reaction. Notably, the peaks at  $1610$  and  $1511\text{ cm}^{-1}$ , which are associated with primary amine groups in glutamic acid, are absent in the GO-GLU 100 sample. This FTIR analysis proves the successful covalent attachment of glutamic acid brushes to the GO nanosheets.

The elemental analysis also revealed the contents of C, H, N and S present in the GO and nanohybrids as shown in Table 3. As the glutamic acid grafting amount increased, similarly its Nitrogen content (3.57%–5.7%). This correlates with the TEM analysis where the dark spots on the GO increased with the increase in glutamic acid amount grafted.

FTIR analysis was performed to identify the chemical composition of virgin PSF, TFC, and TFN membranes (Figure 3c). The FTIR spectra of the pristine PSF membrane exhibited distinct peaks at  $2981$ ,  $1489$ ,  $1293$ , and  $1322\text{ cm}^{-1}$  assigned to aliphatic C-H stretching, C=C stretching within the aromatic ring, S=O stretching, and asymmetric stretching of the C-SO<sub>2</sub>-C group, respectively (Wasim et al., 2017). The aromatic rocking vibrations of C-H peaks can be detected at  $1007$  and  $828\text{ cm}^{-1}$ . Following IP, the TFC and TFN membranes displayed spectra that differed from the virgin PSF membrane. The amide groups (C=O) at  $1675\text{ cm}^{-1}$  are due to an interaction between MPD's amine groups and TMC's acyl chloride groups (Chen et al., 2019). This proves that

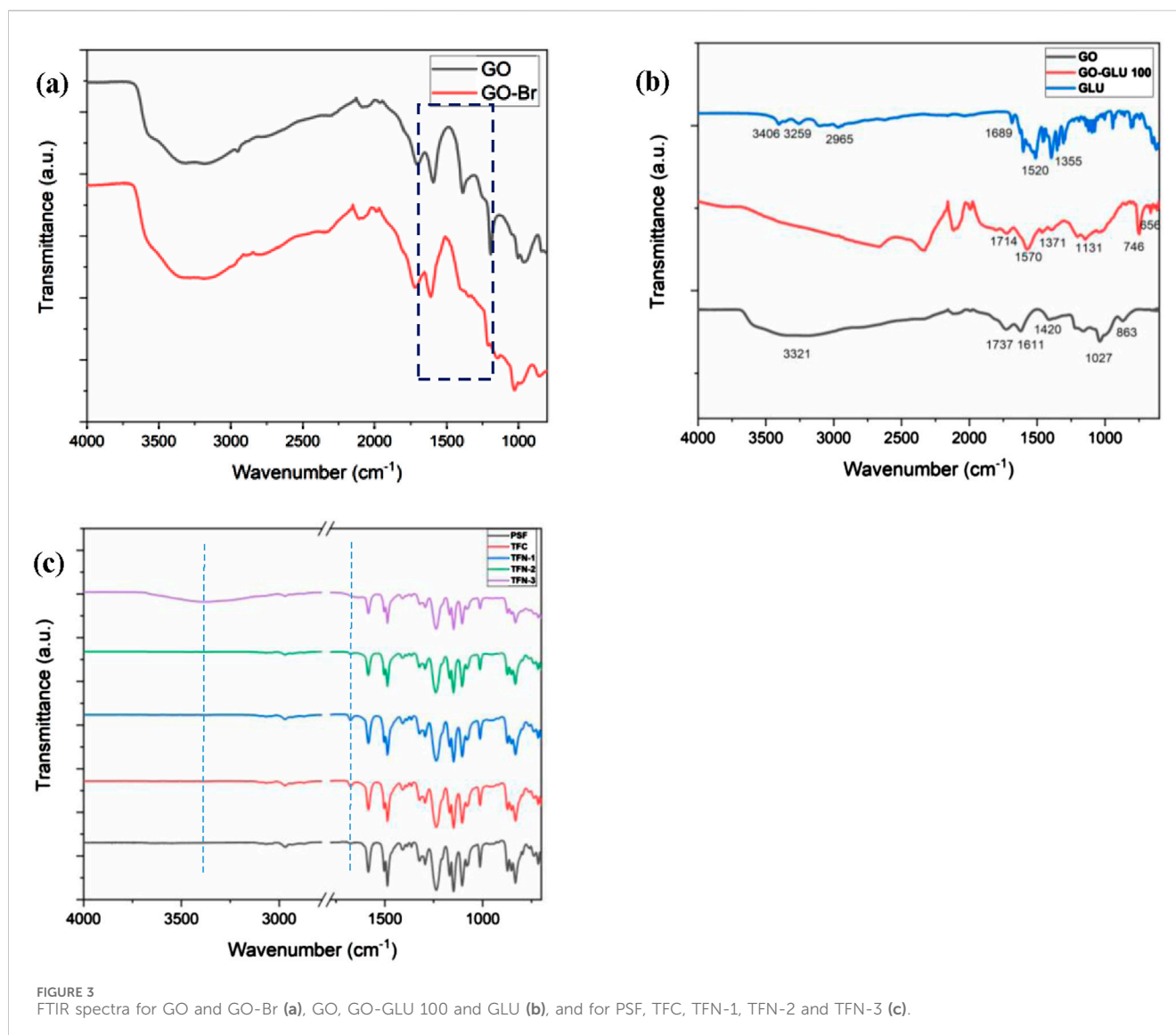


FIGURE 3 FTIR spectra for GO and GO-Br (a), GO, GO-GLU 100 and GLU (b), and for PSF, TFC, TFN-1, TFN-2 and TFN-3 (c).

TABLE 3 Elemental analysis of GO, GO-GLU 50, GO-GLU 100 and GO-GLU 200.

Elements (%)				
Sample	C	H	N	S
GO	37.7	2.894	0	3.783
GO-GLU 50	57.2	2.679	3.57	0.415
GO-GLU 100	56.78	2.804	3.9	0.412
GO-GLU 200	49.9	3.526	5.17	0.223

the PA layer was successfully formed via IP (Chen et al., 2019). Regardless of the GO loading, the TFC and TFN spectra exhibited similar spectra with significant peaks at 1675, 1241 cm<sup>-1</sup> which are credited to C=O (Amide I) and C-N stretch (Wong et al., 2017). Furthermore, TFN-3 exhibits a prominent band at 3372 cm<sup>-1</sup> ascribed to the hydroxyl stretching from the TMCs incomplete hydrolyzed acyl chloride, this also attests to the effective synthesis of the PA layer (Zhao et al., 2018).

### 3.3 TGA, XRD analysis and NMR analysis of GO nanocomposites

Figures 4a,b depicts the TGA of GO and its functionalized hybrids. Functionalized GO displayed a distinct thermal degradation behavior than GO, indicating the successful modification of GO. The GO lost weight in three stages: loss of bound water at 30°C–150°C, decomposition of labile epoxy, carboxylic, and hydroxyl groups (180°C–285°C), and degradation of C-C backbone at ~285°C (Mahmoudian et al., 2018; Namvari et al., 2017). The final mass was approximately 30% of the initial weight. The GO-Br thermal degradation followed a similar trend but its final mass was slightly higher (~40%). This was due to the reduction of oxygenated groups thus less mass loss. Upon glutamic acid brushes grafting, GO-GLU 50 and 100 exhibited higher thermal stabilities with final masses of ~60%. This was attributed to the zwitterions shielding effect on oxygen-containing groups on GO sheets (Xabela and Moutloali, 2022). This also indicates that GO oxygenated functional groups were part of the organo-modification reaction with glutamic acid. However,

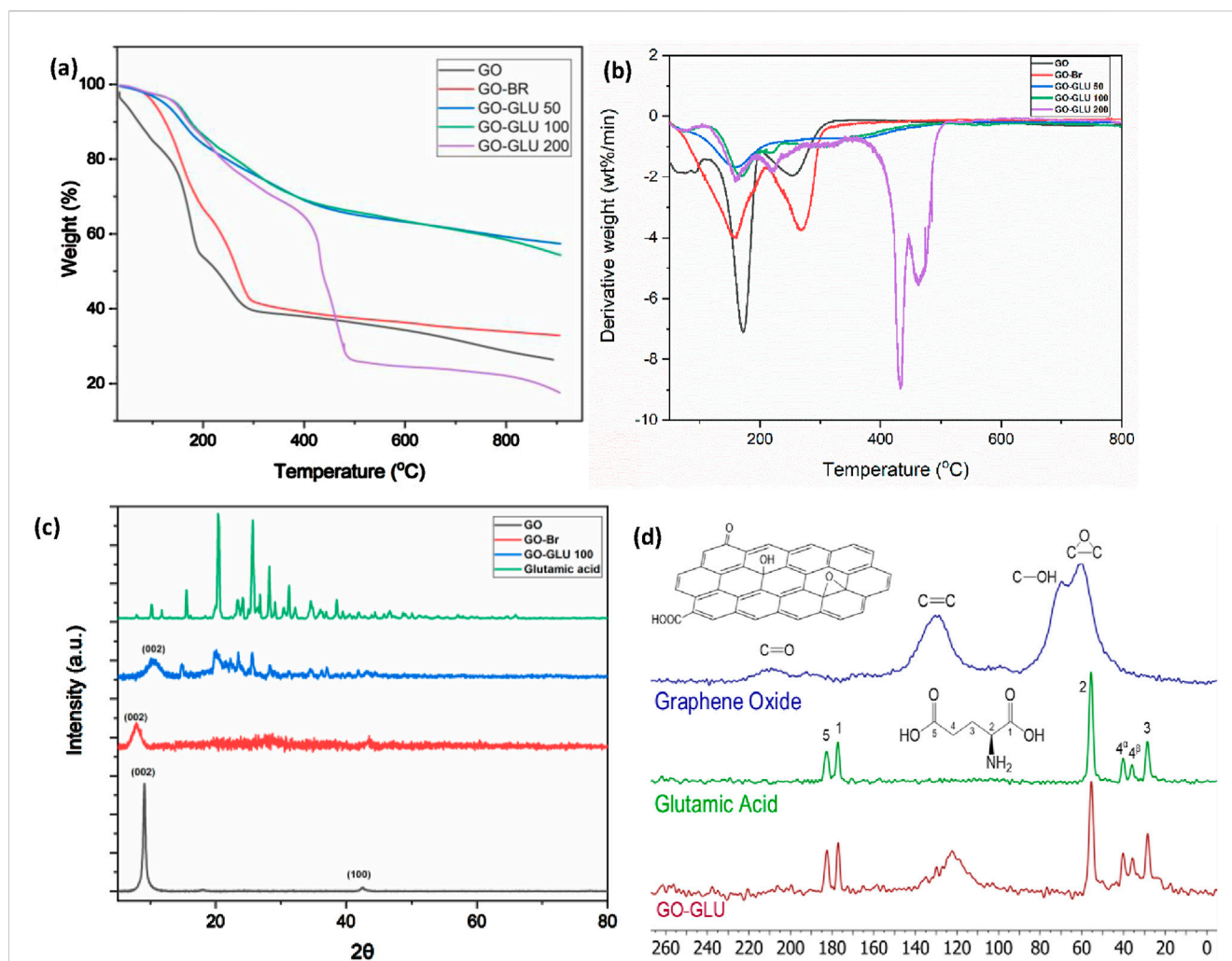


FIGURE 4 TGA thermograms of GO, GO-Br, GO-GLU 50, GO-GLU 100, and GO-GLU (200) (a) and corresponding derivative weight plot (b); XRD patterns of GO, GO-Br, GO-GLU 100 and GLU (c);  $^{13}\text{C}$  MAS NMR spectrum of GO, GLU and GO-GLU (Pulse program = hpdec, MAS = 10 kHz) (d).

with an increase in grafting density, GO-GLU 200 displays thermal instability with a major weight loss at 400°C–500°C and a final mass of ~20%. This is attributable to the lowered van der Waals forces between GO layers as a result of the insertion of polymers between the sheets (Namvari et al., 2017). GO-GLU 100 was chosen as the optimal nanofiller due to its enhanced thermal stability and homogeneous distribution of glutamic acid brushes on GO nanosheets as observed in TEM analysis.

XRD analysis validated the synthesis of GO (Figure 4c). GO diffraction patterns showed peaks at 9.2 and 43 at  $2\theta$  values, representing the (0 0 2) and (1 0 0) GO reflections, respectively. GO's interlayer spacing was 0.96 nm (Gopalakrishnan et al., 2015). The diffraction angle of GO-Br is observed at 7.9° displaying a significant increase in interlayer distance (1.12 nm). This is credited to the reduced intercalated water molecules between the layers due to the decrease in oxygenated functional groups (Xabela and Moutloali, 2022). The XRD pattern for glutamic acid revealed its high crystallization. The GLU polymerized GO displayed a relatively weak peak at 10.5  $2\theta$  indicating an interlayer distance of 0.84 nm prompted by the presence of GLU polymer brushes. The GO-GLU XRD pattern proved the reaction

between the GO and the GLU polymer brushes formed crystal complexes via chemical covalent bonds.

GO contains significant epoxide and hydroxyl functionality as shown by the  $^{13}\text{C}$  MAS NMR spectrum (Figure 4d). Upon grafting with GLU, these peaks seem to be significantly less prominent and an upfield shift is observed for the  $\text{sp}^2$  carbons of the modified GO. Interestingly, the spectrum of GLU shows 2 peaks for the carbon at position 4. This can be attributed to the mixture of  $\alpha$  and  $\beta$  polymorphs that exist in a typical GLU sample. All the carbons are expected to be unique for the  $\alpha$  and  $\beta$  phases, but they are not resolved in this case. The higher resolution  $^{13}\text{C}$  CP MAS NMR spectrum confirms the presence of both  $\alpha$  and  $\beta$  polymorphs with all the signals resolved which is confirmed by the chemical shifts obtained by Wang et al. (2016) (Supplementary Figure S2).

### 3.4 Point of zero charge (PZC)

A substance's PZC in solution is the pH whereby its overall surface charge is zero (Ngaha et al., 2018). The pH PZC of GO-GLU

TABLE 4 Membrane pure water permeation studies.

Membrane	WIC (%)	WCA (°)
TFC	60.11	94.29 ± 5.12
TFN-1	72.63	91.61 ± 6.53
TFN-2	77.64	89.37 ± 6.56
TFN-3	76.55	83.18 ± 5.07

100 was 5.45, meaning at a pH of the solution that exceeds 5.45, the surface charge is negative, neutral at a pH of 5.45, and positive when the pH is less (Supplementary Figure S3) (Borba et al., 2019). Incorporating GO-GLU 100 to the PA layer of membranes will inevitably influence their overall charge. This could indicate that the membrane's pH PZC is close to pH 5.45.

### 3.5 Water permeation studies

The membranes hydrophilicity was assessed using water intake capacity (WIC) and contact angle measurements (Table 4). The TFC membranes' contact angle was higher than the TFN membranes owing to the introduction of GO-GLU 100 in the PA layer. With an increase in GO-GLU 100 (0.025–0.10 wt%) in the PA layer, a decrease in water contact angle was noted (91.61 ± 6.53–83.18 ± 5.07°). The membranes' hydrophilicity was slightly enhanced by the modified GO nanosheets that readily interacted with water molecules thus lowering the contact angle (Shao et al., 2020). This was also confirmed by the WIC which is a bulk hydrophilicity assessment of membranes. The WIC was seen to increase proportionally to the GO-GLU 100 concentration as a result of increase of hydrophilic functional groups per unit area of the membranes. The TFC membrane exhibited the lowest WIC (60.11%) whilst the TFN membranes exhibited higher WIC (72.63%–77.64%).

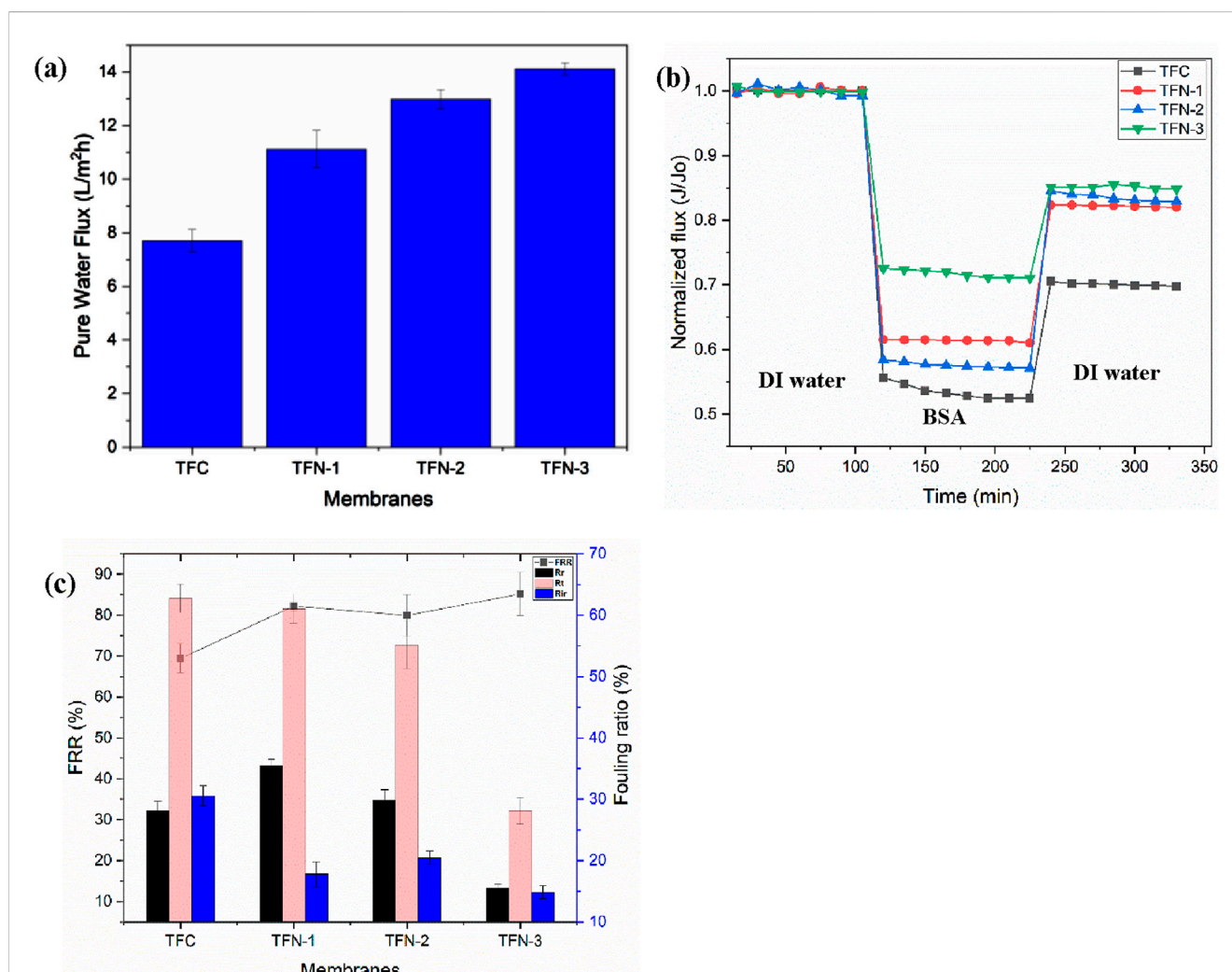
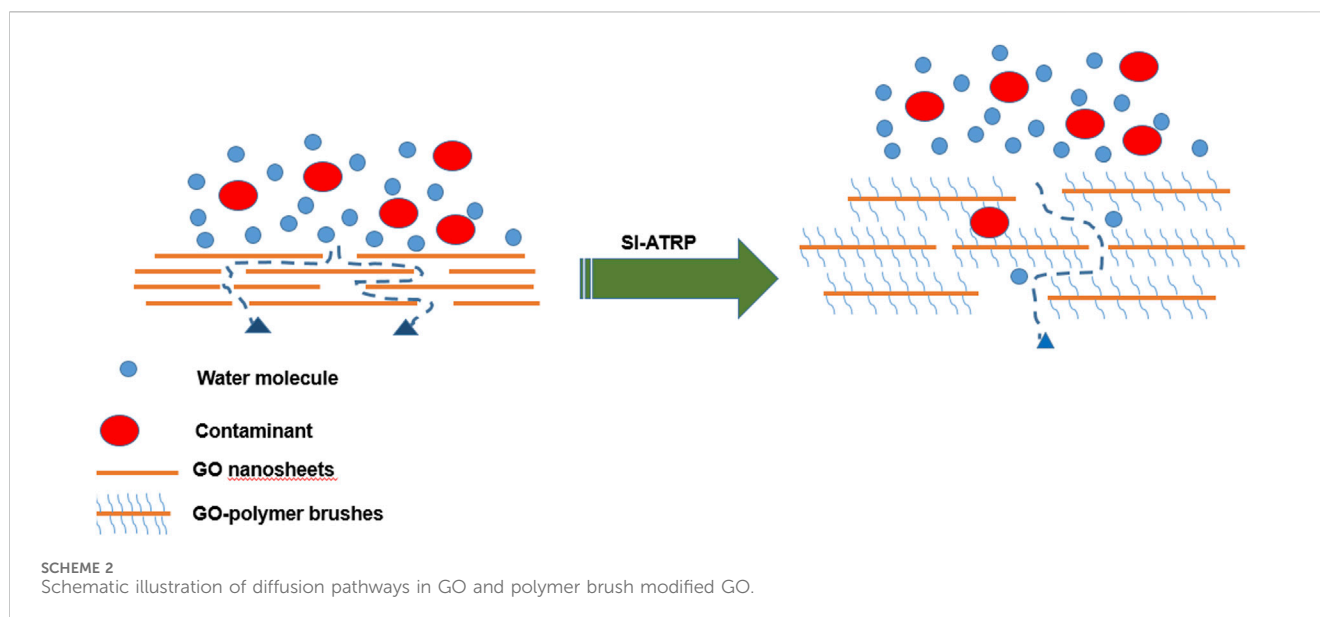


FIGURE 5 Pure water flux of membranes (300 kPa) (a), antifouling experiments for the filtration of BSA; The variation in flux over time (b); and fouling parameters (recovery ratio (FRR), fouling resistance ratios (Rt, Rr, Rir) for different membranes (c).



### 3.6 Membrane filtration properties and antifouling studies

Water permeate flux was utilized to assess the effect of GO-GLU 100 on membrane efficiency (Figure 5). At 300 kPa, the concentration of GO-GLU in the PA layer led to an increase in pure water flux (PWF) from  $7.69 \pm 0.43$  to  $14.11 \pm 0.22$  L/m<sup>2</sup>h. The membranes permeability increased as the nanocomposite increased with TFC having the least PWF and TFN-3 having the highest. The permeability of the membranes is linked to its internal structure and hydrophilicity. This membrane's water permeability and rejection efficacy are determined by the spacing between the layers GO nanosheets coupled with tortuosity of the transport channels. Growing polymer brushes on the GO nanosheets enhanced the lateral and vertical tortuous paths of the GO in the selective PA layer, hence boosting the PWF, as presented in Scheme 2. (Zhang et al., 2022).

Fouling is unavoidable throughout NF operations, owing mostly to the hydrophobic qualities of the surface of NF membrane. The TFN membranes' antifouling characteristics were evaluated using separation experiments with BSA solution (foulant) and pure water as illustrated in.

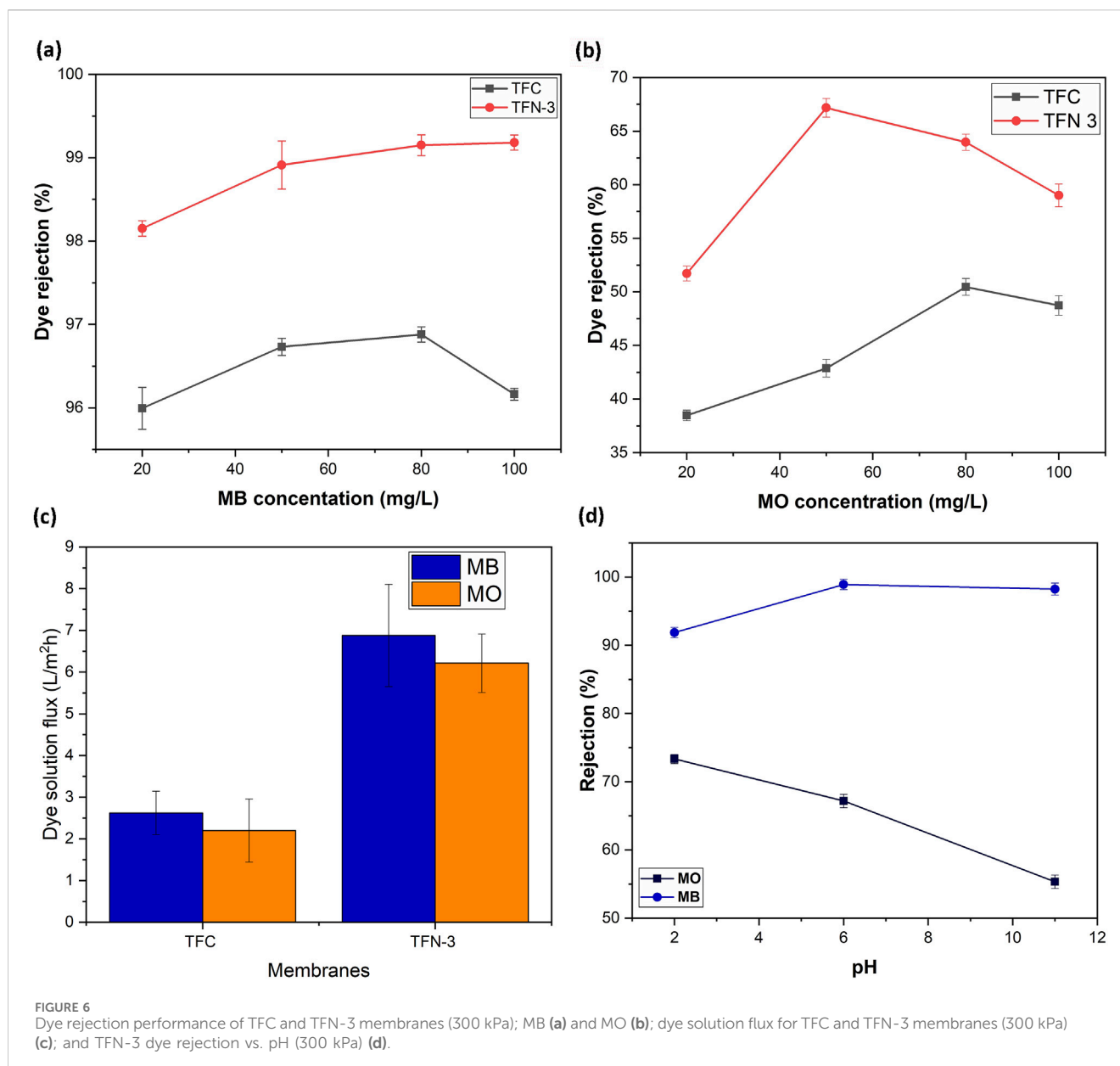
Figures 5b,c. After 120 min running with BSA solution, the permeate fluxes of TFC, TFN-1, TFN-2 and TFN-3 were maintained at ~53%, ~61%, ~57%, and ~72% respectively. The reduction in flux is caused by membrane fouling, which is likely initiated by electrostatic and hydrophobic interactions, Van der Waals forces, and hydrogen bonding forces (Abdulraqeb et al., 2019). TFN membranes had greater BSA normalized flux than TFC membranes. Deionized water was utilized to clean the membranes, and their recovery rates for permeate flux were ~70%, ~82%, ~83% and ~85% respectively. TFN-3 exhibited the best antifouling performance with a recovery normalized flux of ~85%. TFC membranes have a lower flux recovery ratio (FRR) (70.12%) than TFN membranes (79.25%–85.19%). The TFC membrane's fouling resistance ratio,  $R_{ir}$ , was found to be 29.88%. However,  $R_{ir}$  values for TFN membranes were substantially lower

(14.82%–20.79%). The decrease in BSA adsorption onto the surface of the membrane is most probably associated with an increase in the hydrophilicity of TFN membranes. BSA molecules are easily removed by backwashing since foulant-membrane interaction decreases as hydrophilicity increases (Yassari et al., 2022).

### 3.7 Dye rejection studies

#### 3.7.1 Dye concentration effect

To examine the dye removal capabilities of the membranes, tests were performed with varied concentrations of MB and MO (20–100 mg/L). MB and MO represent both cationic and anionic dye categories. This allows for a comprehensive evaluation of the adsorption/rejection performance of the TFN membranes across different charge types. Moreover, MB and MO dyes are prevalent in industrial wastewater, making them a relevant choice for this study. Among all the prepared membranes, TFC and TFN-3 selected for dye removal studies (Figures 6a,b). Table 2 displays the charge and molecular weight (MW) of the dyes under investigation. The surface charge and MW of dye molecules play a critical role in determining their adsorption and/or rejection by TFN membranes. The charge of the dye influences its electrostatic interactions with the membrane surface, thereby affecting whether the dye is retained or allowed to pass through. Meanwhile, the molecular weight dictates the size of the dye molecules relative to the membrane pores, which impacts their ability to be filtered out or permeate through the membrane. Together, these factors are essential for understanding and optimizing the separation performance of TFN membranes. TFC membrane rejection of MB dye ranged from 95.99%–96.87%, whilst TFN-3 rejection ranged from 98.15%–99.18% (Figure 6a). MO dye rejections were lower for both TFC (38.47%–50.46%) and TFN-3 (51.71%–67.18%) (Figure 6b). These results prove that the addition of modified GO nanosheets enhance dye separation owing to a rise in membrane electrostatic charge. The presence of carboxyl groups on the GO-GLU TFN membrane resulted in a negatively charged surface with a high electrostatic affinity to positively charge MB dye



molecules. In contrast, the membrane's negatively charged surface causes electrostatic repulsion towards an anionic dye. Consequently, the cationic dye (MB) displayed better rejection than the anionic dye (MO). Moreover, steric hindrance effects, sieving and the Donnan exclusion principle are useful in explaining the rejection behavior (Goswami et al., 2024). The increased rejection of MB is additionally credited to its larger hydrated radii of 5.04 Å as compared to MOs radii of 4.97 Å that causes sieving hindrances (Sapkota et al., 2020; Akbari et al., 2016). As indicated in Figure 6c, the measured permeate fluxes were lower than those of pure water owing to the dye's sorption on the membrane.

### 3.7.2 Effect of feed solution pH

Similarly, interest was shown in investigating the influence of MB and MO dyes (50 mg/L) on pH-responsive behavior. Membrane separation efficiency can be efficiently altered because solution

pH has a profound effect on the electrochemical characteristics of the dye molecules and membrane surface. Figure 6d shows the pH-responsive separation performance of the dyes. The rate of MB rejection was above 90% at all pH ranges, with pH over 7 improving rejection to 98%. The membrane surface's negative charge lowers at lower pH levels, making it easier for negatively charged MO molecules to adsorb and deposit on it. At pH 2, MO had the highest rejection rate of ~74%. As the solution pH increases, so does the membrane's surface negative charge, and hence MO rejection reduces. Electrostatic repulsion reduced the ability of negatively charged MO dye molecules to adsorb on the membrane surface.

### 3.7.3 Reuse performances

Membrane reusability is critical for practical applications, particularly on a large scale. Accordingly, the membrane's

efficiency and stability is key. As seen in [Supplementary Figure S4](#), the TFN-3 membrane presented excellent rejection performance for both MB and MO dyes (50 mg/L, solution pH) even after three cycles. The removal efficiency of MB dye decreased from 98%–87% whilst MO rejection decreased from 67%–54%. This could be due to membrane fouling or the cleaning process's inability to completely remove absorbed dye molecules. This will eventually lead to a deterioration in the membrane's removal effectiveness.

### 3.8 Dye removal from spiked river water

Spiked river water samples from South Africa's Vaal River were used to examine the possible applicability of the TFN membrane in environmental water systems. The physicochemical characteristics of the water samples were as follows: conductivity 834  $\mu\text{S}/\text{cm}$ , pH 7.61, total dissolved solids (TDS) 417 ppm, and resistivity 1.20  $\text{k}\Omega \text{ cm}$ . The removal efficiencies are presented in [Supplementary Figure S5](#). TFN-3 membrane demonstrated higher removal efficiency for both MB (99.65%) and MO (71.72%) dyes than the control TFC membrane, which removed 95.73% and 49.85% for MB and MO, respectively. The increased removal observed for TFN-3 is due to the synergistic elimination caused by steric hindrance effects, sieving, and Donnan exclusion (Goswami et al., 2024).

### 3.9 Performance comparison of GO-based TFN membranes

[Supplementary Table S1](#) provides a comparative analysis of the performance metrics for GO-based TFN membranes, specifically examining water permeability and dye rejection rates in relation to those developed in this study. Notably, the pressure applied in this research was lower than that typically reported in existing literature. Despite this, the water flux of the GO-GLU incorporated TFN membranes was found to be comparable to that of membranes discussed in previous studies. Most NF membranes operate at significantly higher pressures, which can lead to increased operational costs. The remarkable separation efficiency of the TFN-3 membranes at lower pressure indicates that GO-GLU could be an effective filler material for designing low-pressure TFN NF membranes. This finding highlights the potential for optimizing membrane performance while reducing energy expenditures.

## 4 Conclusion

This study successfully fabricated low pressure TFN membranes by incorporating GO-GLU nanosheets into the PA selective layer via interfacial polymerization. The results demonstrate that GO-GLU significantly enhances membrane hydrophilicity, negative charge density, surface roughness, and antifouling properties. At the optimal GO-GLU dosage of 0.10 wt%, the TFN-3 membrane achieved a water flux of 14.11  $\text{L}/\text{m}^2\text{h}$  at 300 kPa, with superior dye rejection rates of 99.18% for MB and 67.18% for MO. Furthermore, the TFN-3 membrane exhibited excellent antifouling resistance against BSA and maintained stable performance across

three operational cycles. Real-world application testing revealed remarkable dye removal efficiency from river water samples, with rejection rates of 99.65% for MB and 71.75% for MO - outperforming conventional TFC membranes. These results highlight the potential of GO-GLU-based TFN membranes as a promising solution for sustainable wastewater treatment, paving the way for innovative approaches in NF technology.

## Data availability statement

The original contributions presented in the study are included in the article/[Supplementary Material](#), further inquiries can be directed to the corresponding author.

## Author contributions

KM: Conceptualization, Formal Analysis, Investigation, Methodology, Writing – original draft. IK: Investigation, Writing – review and editing. HR: Supervision, Writing – review and editing.

## Funding

The author(s) declare that financial support was received for the research and/or publication of this article. This research was supported by the Volkswagen Foundation (Grant No. 98477).

## Conflict of interest

The authors declare that the research was conducted in the absence of any commercial or financial relationships that could be construed as a potential conflict of interest.

## Generative AI statement

The author(s) declare that no Gen AI was used in the creation of this manuscript.

## Publisher's note

All claims expressed in this article are solely those of the authors and do not necessarily represent those of their affiliated organizations, or those of the publisher, the editors and the reviewers. Any product that may be evaluated in this article, or claim that may be made by its manufacturer, is not guaranteed or endorsed by the publisher.

## Supplementary material

The Supplementary Material for this article can be found online at: <https://www.frontiersin.org/articles/10.3389/frmst.2025.1571459/full#supplementary-material>

## References

- Abadikhah, H., Kalali, E. N., Behzadi, S., Khan, S. A., Xu, X., Shabestari, M. E., et al. (2019b). High flux thin film nanocomposite membrane incorporated with functionalized TiO<sub>2</sub>@reduced graphene oxide nanohybrids for organic solvent nanofiltration. *Chem. Eng. Sci.* 204, 99–109. doi:10.1016/j.ces.2019.04.022
- Abadikhah, H., Kalali, E. N., Khodi, S., Xu, X., and Agathopoulos, S. (2019a). Multifunctional thin-film nanofiltration membrane incorporated with reduced graphene oxide@TiO<sub>2</sub>@Ag nanocomposites for high desalination performance, dye retention, and antibacterial properties. *ACS Appl. Mater. Interfaces* 11 (26), 23535–23545. doi:10.1021/acsami.9b03557
- Abdulraheq, F., Ali, A., Alam, J., Shukla, A. K., Alhoshan, M., Ansari, M. A., et al. (2019). Evaluation of antibacterial and antifouling properties of silver-loaded GO polysulfone nanocomposite membrane against *Escherichia coli*, *Staphylococcus aureus*, and BSA protein. *React. Funct. Polym.* 140, 136–147. doi:10.1016/j.reactfunctpolym.2019.04.019
- Akbari, A., Sheath, P., Martin, S. T., Shinde, D. B., Shaibani, M., Banerjee, P. C., et al. (2016). Large-area graphene-based nanofiltration membranes by shear alignment of discotic nematic liquid crystals of graphene oxide. *Nat. Commun.* 7, 10891. doi:10.1038/ncomms10891
- Anand, A., Unnikrishnan, B., Mao, J. Y., Lin, H. J., and Huang, C. C. (2018). Graphene-based nanofiltration membranes for improving salt rejection, water flux and antifouling—A review. *Desalination* 429, 119–133. doi:10.1016/j.desal.2017.12.012
- Azzaroni, O. (2012). Polymer brushes here, there, and everywhere: recent advances in their practical applications and emerging opportunities in multiple research fields. *J. Polym. Sci. Part A Polym. Chem.* 50 (16), 3225–3258. doi:10.1002/pola.26119
- Bangari, R. S., Yadav, A., Bharadwaj, J., and Sinha, N. (2022). Boron nitride nanosheets incorporated polyvinylidene fluoride mixed matrix membranes for removal of methylene blue from aqueous stream. *J. Environ. Chem. Eng.* 10 (1), 107052. doi:10.1016/j.jece.2021.107052
- Bi, R., Zhang, Q., Zhang, R., Su, Y., and Jiang, Z. (2018). Thin film nanocomposite membranes incorporated with graphene quantum dots for high flux and antifouling property. *J. Memb. Sci.* 553, 17–24. doi:10.1016/j.memsci.2018.02.010
- Borba, L. L., Cuba, R. M. F., Terán, F. J. C., Fj, Castro, M. N., and Mendes, T. A. (2019). Use of adsorbent biochar from pequi (*Caryocar Brasiliense*) husks for the removal of commercial formulation of glyphosate from aqueous media. *Braz. Arch. Biol. Technol.* 62. doi:10.1590/1678-4324-2019180450
- Chen, D., Chen, Q., Liu, T., Kang, J., Xu, R., Cao, Y., et al. (2019). Influence of L-arginine on performances of polyamide thin-film composite reverse osmosis membranes. *RSC Adv.* 9, 20149–20160. doi:10.1039/c9ra02922b
- Cristina, B., Nechifor, A. C., Dimulescu, I. A., Oprea, O., Nechifor, G., Totu, E. E., et al. (2020). Control of nanostructured polysulfone membrane preparation by phase inversion method. *Nanomaterials* 10, 1–20. doi:10.3390/nano10122349
- Etale, A., Nhlane, D., Mhlongo, J., Khan, A., Rumbold, K., Nuapia, Y. B., et al. (2021). Synthesis and application of cationised cellulose for removal of Cr (VI) from acid mine-drainage contaminated water. *AAS Open Res.* 4, 4. doi:10.12688/aasopenres.13182.1
- Feng, X., Peng, D., Zhu, J., Wang, Y., and Zhang, Y. (2022). Recent advances of loose nanofiltration membranes for dye/salt separation. *Sep. Purif. Technol.* 285, 120228. doi:10.1016/j.seppur.2021.120228
- Ge, L., Song, H., Zhu, J., Zhang, Y., Zhou, Z., and Van der Bruggen, B. (2024). Metal/covalent-organic framework based thin film nanocomposite membranes for advanced separations. *J. Mater. Chem. A* 12, 7975–8013. Published online. doi:10.1039/d4ta00578c
- Gopalakrishnan, A., Krishnan, R., Thangavel, S., Venugopal, G., and Kim, S. (2015). Removal of heavy metal ions from pharma-effluents using graphene-oxide nanosorbents and study of their adsorption kinetics. *J. Ind. Eng. Chem.* 30, 14–19. doi:10.1016/j.jiec.2015.06.005
- Goswami, R., Gogoi, M., Borah, A., Sarmah, H., Borah, A. R., Feng, X., et al. (2024). Quantum dot-β-Cyclodextrin nanofiller decorated thin film nanocomposite membrane for removal of cationic and anionic dyes from aqueous solution. *Mater Today Chem.* 35, 101871. doi:10.1016/j.mtchem.2023.101871
- Hebbar, R. S., Isloor, A. M., Prabhu, B., Abdullah, M., Asiri, A. M., and Ismail, A. F. (2018). Removal of metal ions and humic acids through polyetherimide membrane with grafted bentonite clay. *Sci. Rep.* 8, 4665. doi:10.1038/s41598-018-22837-1
- Hoffman, R. (2022). Solid-state chemical-shift referencing with adamantane. *J. Magn. Reson.* 340, 107231. doi:10.1016/j.jmr.2022.107231
- Hu, Z., Li, C., Nie, R., Li, Y., Tang, J., and Deng, X. (2015). Biomaterial functionalized graphene oxides with tunable work function for high sensitive organic photodetectors. *RSC Adv.* 5, 99431–99438. doi:10.1039/c5ra19476h
- Izadmehr, N., Mansourpanah, Y., Ulbricht, M., Rahimpour, A., and Omidkhah, M. R. (2020). TETA-anchored graphene oxide enhanced polyamide thin film nanofiltration membrane for water purification; performance and antifouling properties. *J. Environ. Manage.* 276, 111299. doi:10.1016/j.jenvman.2020.111299
- Jee, H., Jang, J., Kang, Y., Kang, Y., Eisa, T., Chae, K., et al. (2022). Enhancing the dye-rejection efficiencies and stability of graphene oxide-based nanofiltration membranes via divalent cation intercalation and mild reduction. *Membranes* 12 (4), 402. doi:10.3390/membranes12040402
- Kang, Y., Obaid, M., Jang, J., and Kim, I. S. (2019). Sulfonated graphene oxide incorporated thin film nanocomposite nanofiltration membrane to enhance permeation and antifouling properties. *Desalination* 470, 114125. doi:10.1016/j.desal.2019.114125
- Keating, J. J., IV, Imbrogno, J., and Belfort, G. (2016). Polymer brushes for membrane separations: a review. *ACS Appl. Mater. Interfaces* 8, 28383–28399. doi:10.1021/acsami.6b09068
- Kumar, A., Bansal, A., Behera, B., Jain, S. L., and Ray, S. S. (2016). Ternary hybrid polymeric nanocomposites through grafting of polystyrene on graphene oxide-TiO<sub>2</sub> by surface initiated atom transfer radical polymerization (SI-ATRP). *Mater. Chem. Phys.* 172, 189–196. doi:10.1016/j.matchemphys.2016.01.064
- Li, P., Li, Y., Wu, Y., Xu, Z., Zhang, H., Gao, P., et al. (2021). Thin-film nanocomposite NF membrane with GO on macroporous hollow fiber ceramic substrate for efficient heavy metals removal. *Environ. Res.* 197, 111040. doi:10.1016/j.envres.2021.111040
- Li, Q., Li, Y., Ma, X., Du, Q., Sui, K., Wang, D., et al. (2017). Filtration and adsorption properties of porous calcium alginate membrane for methylene blue removal from water. *Chem. Eng. J.* 316, 623–630. doi:10.1016/j.cej.2017.01.098
- Li, Y., Li, C., Li, S., Su, B., Han, L., and Mandal, B. (2019). Graphene oxide (GO)-interlayered thin-film nanocomposite (TFN) membranes with high solvent resistance for organic solvent nanofiltration (OSN). *J. Mater. Chem. A* 7 (21), 13315–13330. doi:10.1039/c9ta01915d
- Liao, Z., Zhu, J., Li, X., and Van der Bruggen, B. (2021). Regulating composition and structure of nanofillers in thin film nanocomposite (TFN) membranes for enhanced separation performance: a critical review. *Sep. Purif. Technol.* 266, 118567. doi:10.1016/j.seppur.2021.118567
- Lin, C. S., Tung, K. L., Lin, Y. L., Dong, D. C., Chen, C. W., and Wu, C. H. (2020). Fabrication and modification of forward osmosis membranes by using graphene oxide for dye rejection and sludge concentration. *Process Saf. Environ. Prot.* 144, 225–235. doi:10.1016/j.psep.2020.07.007
- Ma, D., Peh, S. B., Han, G., and Chen, S. B. (2017). Thin-film nanocomposite (TFN) membranes incorporated with super-hydrophilic metal-organic framework (MOF) UiO-66: toward enhancement of water flux and salt rejection. *ACS Appl. Mater. Interfaces* 9 (8), 7523–7534. doi:10.1021/acsami.6b14223
- Mahmoudian, M., Kochameshki, M. G., and Hosseinzadeh, M. (2018). Modification of graphene oxide by ATRP: a pH-responsive additive in membrane for separation of salts, dyes and heavy metals. *J. Environ. Chem. Eng.* 6 (2), 3122–3134. doi:10.1016/j.jece.2018.04.056
- Mansourpanah, Y., Ghanbari, A., Yazdani, H., Mohammadi, A. G., and Rahimpour, A. (2021). Silver-polyamidoamine/graphene oxide thin film nanofiltration membrane with improved antifouling and antibacterial properties for water purification and desalination. *Desalination* 511, 115109. doi:10.1016/j.desal.2021.115109
- Marcano, D. C., Kosynkin, D. V., Berlin, J. M., Sinitskii, A., Sun, Z., Slesarev, A. S., et al. (2018). Correction to: improved synthesis of graphene oxide. *ACS Nano* 12 (2), 2078. doi:10.1021/acsnano.8b00128
- Masibi, E. G., Makhetha, T. A., and Moutloali, R. M. (2022). Effect of the incorporation of ZIF-8@GO into the thin-film membrane on salt rejection and BSA fouling. *Membranes* 12 (4), 436. doi:10.3390/membranes12040436
- Moradihamedani, P. (2022). Recent advances in dye removal from wastewater by membrane technology: a review. *Polym. Bull.* 79 (4), 2603–2631. doi:10.1007/s00289-021-03603-2
- Mousavi, S. R., Asghari, M., and Mahmoodi, N. M. (2020). Chitosan-wrapped multiwalled carbon nanotube as filler within PEBA thin film nanocomposite (TFN) membrane to improve dye removal. *Carbohydr. Polym.* 237, 116128. doi:10.1016/j.carbpol.2020.116128
- Nair, R. R., Wu, H. A., Jayaram, P. N., Grigorieva, I. V., and Geim, A. K. (2012). Unimpeded permeation of water through helium-leak-tight graphene-based membranes. *Science* 335, 442–444. doi:10.1126/science.1211694
- Namvari, M., Biswas, C. S., Galluzzi, M., Wang, Q., Du, B. B., and Stadler, F. J. (2017). Reduced graphene oxide composites with water soluble copolymers having tailored lower critical solution temperatures and unique tube-like structure. *Nat. Publ. Gr* 7, 44508–44509. doi:10.1038/srep44508
- Natesan, G., and Go, K. R. K. (2023). GO–CuO nanocomposites assimilated into CA–PES polymer membrane in adsorptive removal of organic dyes from wastewater. *Environ. Sci. Pollut. Res.* 30 (15), 42658–42678. doi:10.1007/s11356-022-21821-7
- Ngaha, M. C. D., Djemmoe, L. G., Njanja, E., and Kenfack, I. T. (2018). Biosorption isotherms and kinetics studies for the removal of 2,6-dichlorophenolindophenol using palm tree trunk (*Elaeis guineensis*). *J. Encapsulation Adsorpt. Sci.* 08 (03), 156–177. doi:10.4236/jeas.2018.83008
- Nikooe, N., and Saljoughi, E. (2017). Preparation and characterization of novel PVDF nanofiltration membranes with hydrophilic property for filtration of dye aqueous solution. *Appl. Surf. Sci.* 413, 41–49. doi:10.1016/j.apsusc.2017.04.029
- Ormanci-Acar, T., Celebi, F., Keskin, B., Mutlu-Salmali, O., Agtas, M., Turken, T., et al. (2018). Fabrication and characterization of temperature and pH resistant thin film nanocomposite membranes embedded with halloysite nanotubes for dye rejection. *Desalination* 429, 20–32. doi:10.1016/j.desal.2017.12.005

- Peng, W., Li, H., Liu, Y., and Song, S. (2016). Comparison of Pb (II) adsorption onto graphene oxide prepared from natural graphites: Diagramming the Pb (II) adsorption sites. *Appl. Surf. Sci.* 364, 620–627. doi:10.1016/j.apsusc.2015.12.208
- Pramono, E., Umam, K., Sagita, F., Saputra, O. A., Alfiansyah, R., Dewi, R. S. S., et al. (2023). The enhancement of dye filtration performance and antifouling properties in amino-functionalized bentonite/polyvinylidene fluoride mixed matrix membranes. *Heliyon* 9 (1), e12823. doi:10.1016/j.heliyon.2023.e12823
- Sapkota, B., Liang, W., VahidMohammadi, A., Karnik, R., Noy, A., and Wanunu, M. (2020). High permeability sub-nanometre sieve composite MoS<sub>2</sub> membranes. *Nat. Commun.* 11 (1), 2747–2749. doi:10.1038/s41467-020-16577-y
- Seah, M. Q., Lau, W. J., Goh, P. S., and Ismail, A. F. (2022). Greener synthesis of functionalized-GO incorporated TFN NF membrane for potential recovery of saline water from salt/dye mixed solution. *Desalination* 523, 115403. doi:10.1016/j.desal.2021.115403
- Shakya, J., Mahanta, T., Kumar, S., and Mohanty, T. (2019). Photocatalytic degradation of anionic and cationic dye by using nitrogen doped MoS<sub>2</sub>. *AIP Conf. Proc.* 2115, 030185. doi:10.1063/1.5113024
- Shao, W., Liu, C., Ma, H., Hong, Z., Xie, Q., and Lu, Y. (2019). Fabrication of pH-sensitive thin-film nanocomposite nanofiltration membranes with enhanced performance by incorporating amine-functionalized graphene oxide. *Appl. Surf. Sci.* 487, 1209–1221. doi:10.1016/j.apsusc.2019.05.157
- Shao, W., Liu, C., Yu, T., Xiong, Y., Hong, Z., and Xie, Q. (2020). Constructing positively charged thin-film nanocomposite nanofiltration membranes with enhanced performance. *Polymers* 12, 2526. doi:10.3390/polym12112526
- Tang, K., Zhu, L. S., Lan, P., Chen, Y., Chen, Z., Lan, Y., et al. (2023). Regulating the thickness of nanofiltration membranes for efficient water purification. *Nanoscale Adv.* 5 (18), 4770–4781. doi:10.1039/d3na00110e
- Wang, Y., Wilson, D., and Harbison, G. S. (2016). Solid-state NMR and the crystallization of aspartic and glutamic acids. *Cryst. Growth Des.* 16 (2), 625–631. doi:10.1021/acs.cgd.5b01052
- Wang, Y., Xu, H., Ding, M., Zhang, L., Chen, G., Fu, J., et al. (2022). MXene-regulation polyamide membrane featuring with bubble-like nodule for efficient dye/salt separation and antifouling performance. *RSC Adv.* 12 (17), 10267–10279. doi:10.1039/d2ra00335j
- Wasim, M., Sabir, A., Sha, M., Islam, A., Azam, M., and Jamil, T. (2017). Mixed matrix membranes: two step process modified with electrospun (carboxy methylcellulose sodium salt/sepiolite) fibers for nanofiltration. *J. Ind. Eng. Chem.* 50, 172–182. doi:10.1016/j.jiec.2017.02.011
- Wong, K. C., Goh, P. S., and Ismail, A. F. (2017). Highly permeable and selective graphene oxide-enabled thin film nanocomposite for carbon dioxide separation. *Int. J. Greenh. Gas. Control* 64, 257–266. doi:10.1016/j.ijggc.2017.08.005
- Wu, L., Liu, X., Lv, G., Zhu, R., Tian, L., Liu, M., et al. (2021). Study on the adsorption properties of methyl orange by natural one-dimensional nano-mineral materials with different structures. *Sci. Rep.* 11 (1), 10640–10711. doi:10.1038/s41598-021-90235-1
- Xabela, S., and Moutloali, R. M. (2022). 2-(N-3-Sulfopropyl-N,N-dimethyl ammonium)ethyl methacrylate modified graphene oxide embedded into cellulose acetate ultrafiltration membranes for improved performance. *J. Appl. Polym. Sci.* 139, 1–19. doi:10.1002/app.52336
- Xie, Q., Zhang, S., Xiao, Z., Hu, X., Yi, R., Shao, W., et al. (2017). Preparation and characterization of novel alkali-resistant nanofiltration membranes with enhanced permeation and antifouling properties: the effects of functionalized graphene nanosheets. *RSC Adv.* 7 (30), 18755–18764. doi:10.1039/c7ra00928c
- Yagub, M. T., Sen, T. K., Afroze, S., and Ang, H. M. (2014). Dye and its removal from aqueous solution by adsorption: a review. *Adv. Colloid Interface Sci.* 209, 172–184. doi:10.1016/j.cis.2014.04.002
- Yang, L., Liu, X., Zhang, X., Chen, T., Ye, Z., and Rahaman, M. S. (2022). High performance nanocomposite nanofiltration membranes with polydopamine-modified cellulose nanocrystals for efficient dye/salt separation. *Desalination* 521, 115385. doi:10.1016/j.desal.2021.115385
- Yang, L., Zhang, X., Ma, W., Raisi, B., Liu, X., An, C., et al. (2023). Trimethylamine N-oxide-derived zwitterionic polyamide thin-film composite nanofiltration membranes with enhanced anti-dye deposition ability for efficient dye separation and recovery. *J. Memb. Sci.* 665, 121083. doi:10.1016/j.memsci.2022.121083
- Yang, Y., Wang, J., Zhang, J., Liu, J., Yang, X., and Zhao, H. (2009). Exfoliated graphite oxide decorated by PDMAEMA chains and polymer particles. *Langmuir* 25 (15), 11808–11814. doi:10.1021/la901441p
- Yassari, M., Shakeri, A., Salehi, H., and Reza, S. (2022). Enhancement in forward osmosis performance of thin-film nanocomposite membrane using tannic acid - functionalized graphene oxide. *J. Polym. Res.* 29, 43. doi:10.1007/s10965-022-02894-x
- Zhang, C., Wei, K., Zhang, W., Bai, Y., Sun, Y., and Gu, J. (2017). Graphene oxide quantum dots incorporated into a thin film nanocomposite membrane with high flux and antifouling properties for low-pressure nanofiltration. *ACS Appl. Mater Interfaces* 9 (12), 11082–11094. doi:10.1021/acsami.6b12826
- Zhang, T., Li, P., Ding, S., and Wang, X. (2021). High permeability composite nanofiltration membrane assisted by introducing TpPa covalent organic frameworks interlayer with nanorods for desalination and NaCl/dye separation. *Sep. Purif. Technol.* 270, 118802. doi:10.1016/j.seppur.2021.118802
- Zhang, W., Xu, H., Xie, F., Niu, B., Chen, M., Zhang, H., et al. (2022). General synthesis of ultra fine metal oxide/reduced graphene oxide nanocomposites for ultrahigh-flux nanofiltration membrane. *Nat. Commun.* 13, 471–510. doi:10.1038/s41467-022-28180-4
- Zhao, B., and Zhu, L. (2009). Mixed polymer brush-grafted particles: a new class of environmentally responsive nanostructured materials. *Macromol* 42, 9369–9383. doi:10.1021/ma902042x
- Zhao, D. L., Jin, H., Zhao, Q., Xu, Y., Shen, L., Lin, H., et al. (2023). Smart integration of MOFs and CQDs to fabricate defect-free and self-cleaning TFN membranes for dye removal. *J. Memb. Sci.* 679, 121706. doi:10.1016/j.memsci.2023.121706
- Zhao, G., Hu, R., He, Y., and Zhu, H. (2019b). Physically coating nanofiltration membranes with graphene oxide quantum dots for simultaneously improved water permeability and salt/dye rejection. *Adv. Mater Interfaces* 6 (5), 1–11. doi:10.1002/admi.201801742
- Zhao, P., Li, R., Wu, W., Wang, J., Liu, J., and Zhang, Y. (2019a). *In-situ* growth of polyvinylpyrrolidone modified Zr-MOFs thin-film nanocomposite (TFN) for efficient dyes removal. *Compos Part B Eng.* 176, 107208. doi:10.1016/j.compositesb.2019.107208
- Zhao, W., Liu, H., Meng, N., Jian, M., Wang, H., and Zhang, X. (2018). Graphene oxide incorporated thin film nanocomposite membrane at low concentration monomers. *J. Memb. Sci.* 565, 380–389. doi:10.1016/j.memsci.2018.08.047
- Zhu, S., Li, J., Chen, Y., Chen, Z., Chen, C., Li, Y., et al. (2012). Grafting of graphene oxide with stimuli-responsive polymers by using ATRP for drug release. *J. Nanopart Res.* 14, 1132. doi:10.1007/s11051-012-1132-x